Eur. Phys. J. B **58**, 395–403 (2007)
DOI: 10.1140/epjb/e2007-00251-y

THE EUROPEAN PHYSICAL JOURNAL B

Spin-dependent conductance in FM/quantum-dot/FM tunneling system

L. Qin and Y. Guo[a]

Department of Physics and Key Laboratory of Atomic and Molecular NanoSciences, Ministry of Education, Tsinghua University, Beijing 100084, P.R. China

Received 21 May 2007 / Received in final form 6 August 2007
Published online 22 September 2007

Abstract. We present a theoretical study of the spin-dependent conductance spectra in a FM/semiconductor quantum-dot (QD)/FM system. Both the Rashba spin-orbit (SO) coupling in the QD and spin-flip scattering caused by magnetic barrier impurities are taken into account. It is found that in the single-level QD system with parallel magnetic moments in the two FM leads, due to the interference between different tunneling paths through the spin-degenerate level, a dip or a narrow resonant peak can appear in the conductance spectra, which depends on the property of the spin-flip scattering. When the magnetizations of the two FM leads are noncollinear, the resonant peak can be transformed into a dip. The Rashba SO coupling manifests itself by a Rashba phase factor, which changes the phase information of every tunneling path and can greatly modulate the conductance. When the QD has multiple levels, the Rashba interlevel spin-flip effect appears, which changes the topological property of the structure. Its interplay with the Rashba phase can directly tune the coupling strengths between dot and leads, and can result in switching from resonance into antiresonance in the conductance spectra.

PACS. 72.25.Dc Spin polarized transport in semiconductors – 73.21.La Quantum dots – 73.23.-b Electronic transport in mesoscopic systems

Since the giant magnetoresistance effect (GMR) in magnetic multilayers was discovered [1–3], there has been increasing interest in the field called spintronics [4]. This novel field studies the manipulation of the spin-degree of freedom of electron and in which an important aspect relates to the transport of spin-polarized current in magnetic materials. The spin-dependent transport has already led to lots of new phenomena and devices. For instance, spin-valve effect was discovered in ferromagnet/insulator/ferromagnet structures [5]. GMR was discovered in Fe/Cr multilayers that when a magnetic field is applied, the electric resistance of the magnetic multilayers changes drastically. This is due to the differences in spin-dependent resistivity between the spin-up and spin-down electrons in magnetic multilayers. Applications for GMR structure include many important devices such as magnetic field sensors, read heads for hard drives, and magnetoresistive random access memory, etc.

Nowadays nano-technology allows us to fabricate mesoscopic QD devices [6–11], whose length scale is less than the phase-breaking length, and within which the energy levels are discrete and the quantum mechanism plays an important role. It has potential applications in future quantum computation and quantum information technology. In 1990, Datta and Das proposed a device named Spin Field Effect Transistor [12] (Spin-FET), where the current is modulated by applying a gate voltage to alter the strength of Rashba SO coupling [13]. After the proposal of Spin-FET, lots of research work has focused on it and the Rashba SO coupling caused by structure inversion asymmetry also gains much attention, because its strength can be tuned over a wide range by the external field [14,15]. Recent discovery of intrinsic spin-Hall effect in p-doped semiconductors by Murakami et al. [16] and in Rashba SO coupled two-dimensional electron gas (2DEG) by Sinova et al. [17] may develop a new way to effectively generate spin-polarized current in paramagnetic semiconductors, which is the fundamental condition of realizing spintronics devices.

In this paper we investigate transport properties of a FM/QD/FM tunneling system [18–22] sketched in Figure 1a, where the QD is made of 2DEG, and electrons are confined in the y direction, which leads to a finite Rashba SO coupling [23]. Here we neglect the Coulomb interaction in the QD in order to get a clear insight into the physics of this system. Owing to the magnetic barrier impurities, spin-flip scattering can occur during the tunneling

[a] e-mail: guoy66@tsinghua.edu.cn

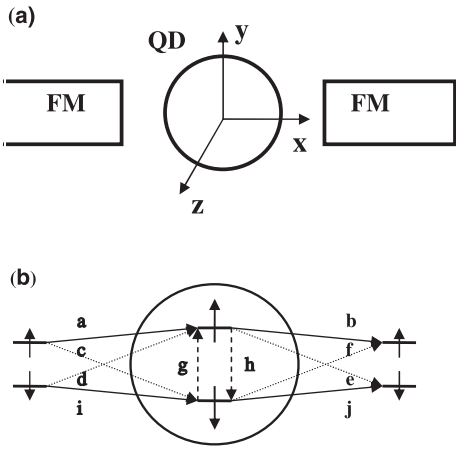

Fig. 1. (a) The tunneling system with ferromagnetic leads coupled to a semiconductor QD. The QD is made of 2DEG which is confined in the y axis. Electrons transport along the x direction. (b) The figure sketches different tunneling paths between the two FM leads for spin-up and spin-down electrons.

process [24,25], which introduces more paths for electrons tunneling through the structure.

We model the system with the Hamiltonian $H = H_d + \sum_\alpha H_\alpha + \sum_\alpha H_{T\alpha}, \alpha = L, R$. Here H_α describes the αth FM lead and can be written as $H_\alpha = \sum_{k_\alpha\sigma} \varepsilon_{k_\alpha\sigma} a^\dagger_{k_\alpha\sigma} a_{k_\alpha\sigma}$, where $a^\dagger_{k_\alpha\sigma}$ ($a_{k_\alpha\sigma}$) is the creation (annihilation) operator of electron in lead α with wave vector k and spin σ (quantized along the magnetic moment of lead α). The Hamiltonian of the QD in the absence of Rashba SO interaction is $H_d = \sum_{n\sigma} \varepsilon_{n\sigma} d^\dagger_{n\sigma} d_{n\sigma}$, and the corresponding tunneling Hamiltonian between the QD and the αth lead is [24,26]

$$H_{T\alpha} = \sum_{k_\alpha n\sigma\sigma'} [T^{\sigma\sigma'}_{k_\alpha n}(\cos\frac{\theta_\alpha}{2} a^\dagger_{k_\alpha\sigma} - \sigma \sin\frac{\theta_\alpha}{2} a^\dagger_{k_\alpha\bar{\sigma}}) d_{n\sigma'} + H.c.], \tag{1}$$

where $\sigma = \uparrow$ and $\downarrow$ correspond to $\sigma = \pm 1$, $\bar{\sigma} = -\sigma$, θ_α is the relative angle between the magnetic moment of the αth lead and the spin quantization axis on the dot (z axis), $d^\dagger_{n\sigma}$ ($d_{n\sigma}$) is the creation (annihilation) operator of electron on the nth level of the dot with spin σ, and $T^{\sigma\sigma'}_{k_\alpha n}$ are the dot-lead coupling matrix elements, which are assumed to be real numbers in this work. Now we take into account the Rashba SO interaction in the QD, which can be written as [23]

$$\begin{aligned} H_{SO} &= \frac{1}{2\hbar}[\alpha(x)\hat{\sigma}_z p_x - \hat{\sigma}_z p_x \alpha(x)] - \alpha(x)\hat{\sigma}_x p_z/\hbar \\ &\equiv H_{R1} + H_{R2}. \end{aligned} \tag{2}$$

Here $\alpha(x)$ is the Rashba SO coupling parameter. For electrons transport along the x axis, H_{R1} causes the spin-precession, while H_{R2} causes the spin-flipping, which is similar to the intersubband mixing effect. According to reference [23], after a unitary transformation U, H_{R1} disappears with only a phase factor $e^{-i\sigma'\phi^\alpha_{so}}$ left, which multiplies on the tunneling coefficient $T^{\sigma\sigma'}_{k_\alpha n}$. Here we have $\phi^L_{so} = 0$ and $\phi^R_{so} = \int_{x_L}^{x_R} k_R(x)dx \equiv \phi_{so}$, where $k_R(x) = \alpha(x)m^*/\hbar^2$. If we assume $\alpha(x)$ is independent of x, then $\phi_{so} = \alpha m^* L/\hbar^2$ with L the length of the dot. After the transformation, H_{R2} can be written as $H_{R2} = \sum_{m,n} t_{mn} d^\dagger_{m\downarrow} d_{n\uparrow} + H.c.$, where $t_{mn} \equiv \langle m\downarrow | U^\dagger H_{R2} U | n\uparrow\rangle$ and $t_{mn} = -t_{nm}$ ($t_{nn} = 0$), which means that Rashba SO coupling only induces interlevel spin-flipping rather than intralevel spin-flipping. Both ϕ_{so} and t_{mn} are proportional to α. In reference [23] the authors had estimated the magnitudes of ϕ_{so} and t_{mn}. They showed that ϕ_{so} could be tuned to $\pi/2$ experimentally, and t_{mn} has the typical magnitude of 100 μeV, which can be the same with the magnitudes of the coupling strength and level separation. Because other parts of the Hamiltonian remains unchanged under the transformation, we can rewrite the Hamiltonian in the presence of Rashba SO interaction as

$$H_d = \sum_{n\sigma} \varepsilon_{n\sigma} d^\dagger_{n\sigma} d_{n\sigma} + \sum_{mn} (t_{mn} d^\dagger_{m\downarrow} d_{n\uparrow} + H.c.), \tag{3}$$

and

$$H_{T\alpha} = \sum_{k_\alpha n\sigma\sigma'} (\widetilde{T}^{\sigma\sigma'}_{k_\alpha n} a^\dagger_{k_\alpha\sigma} d_{n\sigma'} + H.c.), \tag{4}$$

where

$$\begin{aligned} \widetilde{T}^{\uparrow\uparrow}_{k_\alpha n} &= (T^{\uparrow\uparrow}_{k_\alpha n}\cos\frac{\theta_\alpha}{2} + T^{\downarrow\uparrow}_{k_\alpha n}\sin\frac{\theta_\alpha}{2}) e^{-i\phi^\alpha_{so}}, \\ \widetilde{T}^{\uparrow\downarrow}_{k_\alpha n} &= (T^{\downarrow\downarrow}_{k_\alpha n}\sin\frac{\theta_\alpha}{2} + T^{\uparrow\downarrow}_{k_\alpha n}\cos\frac{\theta_\alpha}{2}) e^{i\phi^\alpha_{so}}, \\ \widetilde{T}^{\downarrow\uparrow}_{k_\alpha n} &= (-T^{\uparrow\uparrow}_{k_\alpha n}\sin\frac{\theta_\alpha}{2} + T^{\downarrow\uparrow}_{k_\alpha n}\cos\frac{\theta_\alpha}{2}) e^{-i\phi^\alpha_{so}}, \\ \widetilde{T}^{\downarrow\downarrow}_{k_\alpha n} &= (T^{\downarrow\downarrow}_{k_\alpha n}\cos\frac{\theta_\alpha}{2} - T^{\uparrow\downarrow}_{k_\alpha n}\sin\frac{\theta_\alpha}{2}) e^{i\phi^\alpha_{so}}. \end{aligned} \tag{5}$$

For simplicity, we assume $T^{\sigma\sigma'}_{k_\alpha n}$ to be independent of wave vector k_α and rewrite them as $T^{\uparrow\uparrow}_{k_\alpha n} = T^\alpha_{n1}$, $T^{\downarrow\downarrow}_{k_\alpha n} = T^\alpha_{n2}$, $T^{\uparrow\downarrow}_{k_\alpha n} = T^\alpha_{n3}$, and $T^{\downarrow\uparrow}_{k_\alpha n} = T^\alpha_{n4}$, and replace the subscript k_α in $\widetilde{T}^{\sigma\sigma'}_{k_\alpha n}$ by α. In this work we set $T^\alpha_{n1} = T^\alpha_{n2}$ except in Figures 5c and 5d, and we denote both of them by T^α_{n1}. T^α_{n3} and T^α_{n4} describe the spin-flip tunneling process, and their values depend on the property of the magnetic barrier impurities. Here we assume T^α_{n3} and T^α_{n4} to be lesser than T^α_{n1}, which means that the spin states of most electrons are not affected by the impurities during the tunneling process.

Within the standard Green function technique [27] the expression of the spin-dependent current can be written as

$$I^\alpha_\sigma = -\frac{2e}{\hbar}\mathrm{Im}\int \frac{d\varepsilon}{2\pi} Tr[(G^r(\varepsilon) f_\alpha(\varepsilon) + \frac{1}{2}G^<(\varepsilon))\Gamma^{\alpha\sigma}]. \tag{6}$$

Without loss of generality, in the following we investigate the current flowing out of the left lead. After some algebra we gain the expression of the spin-dependent linear

conductance in zero temperature limit as follows

$$G^{\sigma} = \frac{e^2}{h} Tr(G^r \Gamma^R G^a \Gamma^{L\sigma}). \tag{7}$$

Here $G^{r(a)}$ and $\Gamma^{\alpha}(=\Gamma^{\alpha\uparrow}+\Gamma^{\alpha\downarrow})$ are the retarded (advanced) Green function of the dot and the coupling matrix between the dot and the αth lead, respectively. Both $G^{r(a)}$ and $\Gamma^{\alpha\sigma}$ are $2n\times 2n$ matrices, where n is the number of energy levels in the QD. They can also be taken as $n\times n$ matrices, whose elements, $G^{r(a)}_{nn'}$ and $\Gamma^{\alpha\sigma}_{nn'}$, are 2×2 matrices in spin space. $G^r_{nn'}$ has the expression

$$G^r_{nn'} = \begin{pmatrix} G^{r\uparrow\uparrow}_{nn'} & G^{r\uparrow\downarrow}_{nn'} \\ G^{r\downarrow\uparrow}_{nn'} & G^{r\downarrow\downarrow}_{nn'} \end{pmatrix}, \tag{8}$$

where $G^{r\sigma\sigma'}_{nn'} = \ll d^{\dagger}_{n\sigma} \mid d_{n'\sigma'} \gg^r$, and $G^a_{nn} = [G^r_{n'n}]^{\dagger}$. $\Gamma^{\alpha\sigma}_{nn'}$ has the expression

$$\Gamma^{\alpha\sigma}_{nn'} = \sum_{k_\alpha} 2\pi\delta(\omega-\varepsilon_{k_\alpha\sigma}) \begin{pmatrix} \widetilde{T}^{\sigma\uparrow *}_{\alpha n}\widetilde{T}^{\sigma\uparrow}_{\alpha n'} & \widetilde{T}^{\sigma\uparrow *}_{\alpha n}\widetilde{T}^{\sigma\downarrow}_{\alpha n'} \\ \widetilde{T}^{\sigma\downarrow *}_{\alpha n}\widetilde{T}^{\sigma\uparrow}_{\alpha n'} & \widetilde{T}^{\sigma\downarrow *}_{\alpha n}\widetilde{T}^{\sigma\downarrow}_{\alpha n'} \end{pmatrix}. \tag{9}$$

Here we have $\sum\limits_{k_\alpha}\delta(\omega-\varepsilon_{k_\alpha\sigma}) = \rho_{\alpha\sigma}$, $\rho_{\alpha\uparrow}+\rho_{\alpha\downarrow} = \rho_{\alpha}$, and $P_\alpha = (\rho_{\alpha\uparrow}-\rho_{\alpha\downarrow})/\rho_\alpha$, where $\rho_{\alpha\sigma}$ and P_α are the spin-dependent density of states and spin-polarization rate in the αth lead, respectively. For convenience, we denote $2\pi\rho_\alpha T^{\alpha}_{ni}T^{\alpha}_{n'j}$ by $T^{\alpha}_{ni}T^{\alpha}_{n'j}$ $(i,j=1,2,3,4)$ in this manuscript. $P_L = P_R = P > 0$ is assumed in this work, i.e., the spin-up electrons dominant. Then the elements of $\Gamma^{\alpha\uparrow}_{nn'}$ and $\Gamma^{\alpha\downarrow}_{nn'}$ can be explicitly written as

$$\begin{aligned}
\Gamma^{\alpha\uparrow}_{nn'}(1,1) &= \frac{1+P}{2}\left(T^{\alpha}_{n1}\cos\frac{\theta_\alpha}{2}+T^{\alpha}_{n4}\sin\frac{\theta_\alpha}{2}\right) \\
&\quad\times\left(T^{\alpha}_{n'1}\cos\frac{\theta_\alpha}{2}+T^{\alpha}_{n'4}\sin\frac{\theta_\alpha}{2}\right), \\
\Gamma^{\alpha\uparrow}_{nn'}(1,2) &= \frac{1+P}{2}\left(T^{\alpha}_{n1}\cos\frac{\theta_\alpha}{2}+T^{\alpha}_{n4}\sin\frac{\theta_\alpha}{2}\right) \\
&\quad\times\left(T^{\alpha}_{n'2}\sin\frac{\theta_\alpha}{2}+T^{\alpha}_{n'3}\cos\frac{\theta_\alpha}{2}\right)e^{2i\phi^{\alpha}_{so}}, \\
\Gamma^{\alpha\uparrow}_{nn'}(2,1) &= \frac{1+P}{2}\left(T^{\alpha}_{n2}\sin\frac{\theta_\alpha}{2}+T^{\alpha}_{n3}\cos\frac{\theta_\alpha}{2}\right) \\
&\quad\times\left(T^{\alpha}_{n'1}\cos\frac{\theta_\alpha}{2}+T^{\alpha}_{n'4}\sin\frac{\theta_\alpha}{2}\right)e^{-2i\phi^{\alpha}_{so}}, \\
\Gamma^{\alpha\uparrow}_{nn'}(2,2) &= \frac{1+P}{2}\left(T^{\alpha}_{n2}\sin\frac{\theta_\alpha}{2}+T^{\alpha}_{n3}\cos\frac{\theta_\alpha}{2}\right) \\
&\quad\times\left(T^{\alpha}_{n'2}\sin\frac{\theta_\alpha}{2}+T^{\alpha}_{n'3}\cos\frac{\theta_\alpha}{2}\right),
\end{aligned} \tag{10}$$

and

$$\begin{aligned}
\Gamma^{\alpha\downarrow}_{nn'}(1,1) &= \frac{1-P}{2}\left(-T^{\alpha}_{n1}\sin\frac{\theta_\alpha}{2}+T^{\alpha}_{n4}\cos\frac{\theta_\alpha}{2}\right) \\
&\quad\times\left(-T^{\alpha}_{n'1}\sin\frac{\theta_\alpha}{2}+T^{\alpha}_{n'4}\cos\frac{\theta_\alpha}{2}\right), \\
\Gamma^{\alpha\downarrow}_{nn'}(1,2) &= \frac{1-P}{2}\left(-T^{\alpha}_{n1}\sin\frac{\theta_\alpha}{2}+T^{\alpha}_{n4}\cos\frac{\theta_\alpha}{2}\right) \\
&\quad\times\left(T^{\alpha}_{n'2}\cos\frac{\theta_\alpha}{2}-T^{\alpha}_{n'3}\sin\frac{\theta_\alpha}{2}\right)e^{2i\phi^{\alpha}_{so}}, \\
\Gamma^{\alpha\downarrow}_{nn'}(2,1) &= \frac{1-P}{2}\left(T^{\alpha}_{n2}\cos\frac{\theta_\alpha}{2}-T^{\alpha}_{n3}\sin\frac{\theta_\alpha}{2}\right) \\
&\quad\times\left(-T^{\alpha}_{n'1}\sin\frac{\theta_\alpha}{2}+T^{\alpha}_{n'4}\cos\frac{\theta_\alpha}{2}\right)e^{-2i\phi^{\alpha}_{so}}, \\
\Gamma^{\alpha\downarrow}_{nn'}(2,2) &= \frac{1-P}{2}\left(T^{\alpha}_{n2}\cos\frac{\theta_\alpha}{2}-T^{\alpha}_{n3}\sin\frac{\theta_\alpha}{2}\right) \\
&\quad\times\left(T^{\alpha}_{n'2}\cos\frac{\theta_\alpha}{2}-T^{\alpha}_{n'3}\sin\frac{\theta_\alpha}{2}\right).
\end{aligned} \tag{11}$$

With the equation of motion method we get $G^r(\omega) = [A(\omega)-R+i\Gamma/2]^{-1}$, where

$$\begin{aligned}
A_{nn'}(\omega) &= \delta_{nn'}\begin{pmatrix} \omega-\varepsilon_{n\uparrow} & 0 \\ 0 & \omega-\varepsilon_{n\downarrow}\end{pmatrix}, \\
R_{nn'} &= \begin{pmatrix} 0 & t^*_{n'n} \\ t_{nn'} & 0\end{pmatrix},
\end{aligned} \tag{12}$$

and $\Gamma = \Gamma^L + \Gamma^R$. The Rashba spin-precession manifests itself by the phase factor $e^{\pm 2i\phi_{so}}$ in matrix Γ, while the Rashba interlevel spin-flip effect is manifested by the matrix R. In this work we focus on two situations. One is the QD with one energy level $(n=1)$, the other is the QD with two levels $(n=2)$, which can be spin-degenerate or non-degenerate. In the former case the matrix R vanishes because $t_{nn'}$ doesn't have diagonal components, and here we present the expression of G^r as follows:

$$\begin{aligned}
\mathbf{G^r}(\omega) &= \begin{pmatrix} \omega-\varepsilon_{0\uparrow}+\frac{i}{2}\Gamma_{11} & \frac{i}{2}\Gamma_{12} \\ \frac{i}{2}\Gamma_{21} & \omega-\varepsilon_{0\downarrow}+\frac{i}{2}\Gamma_{22}\end{pmatrix}^{-1} \\
&= \frac{1}{|G|}\begin{pmatrix} \omega-\varepsilon_{0\downarrow}+\frac{i}{2}\Gamma_{22} & -\frac{i}{2}\Gamma_{12} \\ -\frac{i}{2}\Gamma_{21} & \omega-\varepsilon_{0\uparrow}+\frac{i}{2}\Gamma_{11}\end{pmatrix},
\end{aligned} \tag{13}$$

where $|G| = (\omega-\varepsilon_{0\uparrow}+i\Gamma_{11}/2)(\omega-\varepsilon_{0\downarrow}+i\Gamma_{22}/2)+\Gamma_{12}\Gamma_{21}/4$. In the case of a two-level QD $t_{12}(=-t_{21})$ are finite, and we assume $t_{12}(=t)$ is a real quantity, which represents the strength of Rashba interlevel spin-flip effect. Our discussion is also valid in multilevel systems provided that the energy level separation is much larger than the coupling strength, because then the transport properties at one resonant level are mainly affected by the nearby level, and the influences from other levels are negligible. In the strong coupling limit, the influences from all levels are needed to be considered when we investigate the conductance spectra at one energy level, and the situation becomes much more complex, which is beyond the scope of our discussion.

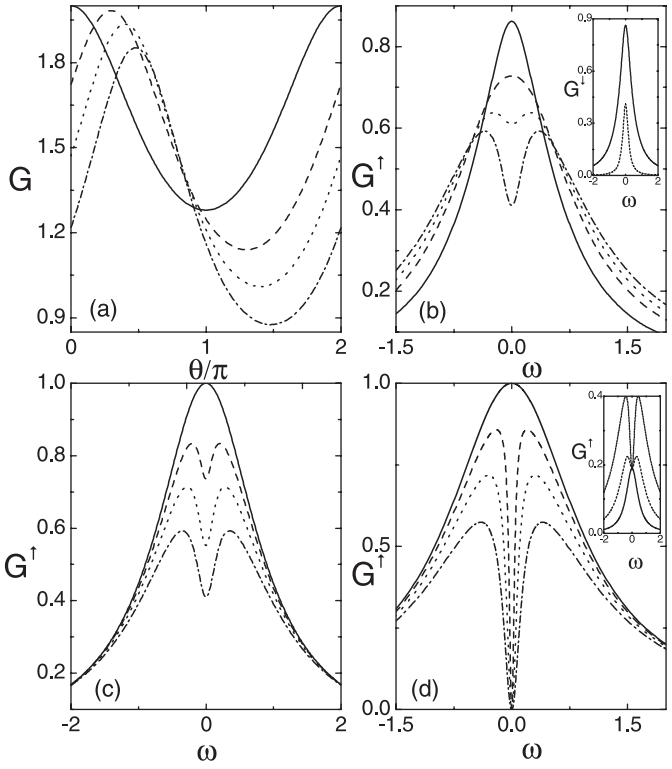

Fig. 2. The linear conductance G and G^σ for different sets of parameters assuming only spin-flip scattering in the left barrier ($T_4^L = T_3^R = T_4^R = 0$) and absent Rashba SO coupling in the dot. (a) Dependence of the total conductance on the relative magnetization angle θ of the two leads for different T_3^L parameters and fixed lead polarization $P = 0.8$. (b) Energy-resolved $G^\uparrow$ for different lead polarizations P in the case of parallel leads ($\theta_L = \theta_R = 0$) and fixed $T_3^L = 0.8$. The inset shows the corresponding situation for $G^\downarrow$ for $P = 0.2$ and $P = 0.8$, respectively. (c) $G^\uparrow$ for different T_3^L parameters in the case of parallel leads and $P = 0.8$ and (d) $P = 1$, respectively. The inset of (d) shows the corresponding situation for antiparallel leads configuration for $T_3^L = 0, 0.4$, and 0.8, respectively. The solid, dashed, dotted, and dash-dotted lines in (a), (c), and (d) correspond to $T_3^L = 0, 0.4, 0.6$, and 0.8, and in (b) correspond to $P = 0, 0.4, 0.6$, and 0.8, respectively. For all figures $\varepsilon_0 = 0$ and $T_1^L = T_1^R = 1$ are assumed.

First we study the case that the dot has one energy level, which is assumed to be spin-degenerate ($\varepsilon_\uparrow = \varepsilon_\downarrow$). In this situation we omit the subscript n in all formulas. From the expression of $\Gamma^{\alpha\sigma}$ we know that even when $\theta_L = \theta_R = 0$, the off-diagonal elements of $\Gamma^{\alpha\sigma}$ are finite, provided that T_3^α or T_4^α is non-zero. This indicates that T_3^α and T_4^α have the effect to rotate the direction of the magnetization of the αth FM lead, and can be understood as follows. Owing to the spin-flip effect, electrons can tunnel onto both spin-up and down states in the dot, which is similar to the case that the magnetizations of the two leads are noncollinear. The phenomenon is revealed in Figure 2a, which shows the conductance (in the unit of e^2/h) as a function of the relative angle between the two leads. For $T_3^L = 0$, G decreases monotonously as θ varies from 0 to π, which is the normal TMR effect. When T_3^L is finite, the magnetization of the left lead has been essentially rotated, so G first increases and then decreases with θ. We can also see that with the introduction of spin-flip effect, the conductance has been suppressed. So the spin-flip effect has some other influences on the transport property, which will be investigated below.

Now we consider a simple situation that the magnetizations of the two leads are parallel and the Rashba SO coupling is absent. To get a clear physics picture we take into account the spin-flip effect by choosing only T_3^L to be finite. Figures 2b–2d show the spin-dependent conductance spectra for different parameters. In Figure 2b, when the polarization rate P is small, $G^\uparrow$ shows a resonant peak at the spin-degenerate level ε_0, while as P increases, the peak reduces to a dip. At the non-resonant energy region, $G^\uparrow$ increases with P. In the inset we can see $G^\downarrow$ always shows a peak at ε_0, and its value is suppressed by P. In Figure 2c we plot $G^\uparrow$ for different values of T_3^L. When $T_3^L = 0$, the conductance reaches the full transmission, and with T_3^L increasing, the conductance is reduced, while a dip appears and the peak is split into two lower peaks with equal height. So we conclude that when T_3^L is finite, the resonant peak of $G^\uparrow$ at ε_0 can be transformed into a dip, provided that P and T_3^L are large enough, while in the spectra of $G^\downarrow$ the resonant peak always exists. This is different from the case when spin-flip effect is absent, where there is always a resonant peak at ε_0 in the spectra of both $G^\uparrow$ and $G^\downarrow$. These characteristics can be understood as follows. From equation (7), we have

$$G^\sigma = \left|T_1^\sigma + T_2^\sigma + T_3^\sigma + T_4^\sigma\right|^2 + \left|T_5^\sigma + T_6^\sigma + T_7^\sigma + T_8^\sigma\right|^2, \quad (14)$$

where

$$\begin{aligned}
T_1^\sigma &= G^{r\uparrow\uparrow}\sqrt{\Gamma_{11}^{R\uparrow}\Gamma_{11}^{L\sigma}}e^{i\phi_{so}},\\
T_2^\sigma &= G^{r\downarrow\downarrow}\sqrt{\Gamma_{22}^{R\uparrow}\Gamma_{22}^{L\sigma}}e^{-i\phi_{so}},\\
T_3^\sigma &= G^{r\downarrow\uparrow}\sqrt{\Gamma_{11}^{R\uparrow}\Gamma_{22}^{L\sigma}}e^{i\phi_{so}},\\
T_4^\sigma &= G^{r\uparrow\downarrow}\sqrt{\Gamma_{22}^{R\uparrow}\Gamma_{11}^{L\sigma}}e^{-i\phi_{so}},\\
T_5^\sigma &= G^{r\uparrow\uparrow}\sqrt{\Gamma_{11}^{R\downarrow}\Gamma_{11}^{L\sigma}}e^{i\phi_{so}},\\
T_6^\sigma &= G^{r\downarrow\downarrow}\sqrt{\Gamma_{22}^{R\downarrow}\Gamma_{22}^{L\sigma}}e^{-i\phi_{so}},\\
T_7^\sigma &= G^{r\downarrow\uparrow}\sqrt{\Gamma_{11}^{R\downarrow}\Gamma_{22}^{L\sigma}}e^{i\phi_{so}},\\
T_8^\sigma &= G^{r\uparrow\downarrow}\sqrt{\Gamma_{22}^{R\downarrow}\Gamma_{11}^{L\sigma}}e^{-i\phi_{so}}. \qquad (15)
\end{aligned}$$

Here $\Gamma_{ij}^{\alpha\sigma} = \Gamma^{\alpha\sigma}(i,j)$. These quantities are the transmission amplitudes for electron with spin σ tunnels from the left lead to the right one through different paths. Taking $G^\uparrow$ for example. As depicted in Figure 1b, $T_1^\uparrow$ is the transmission amplitude via tunneling path ab, and $T_3^\uparrow$ is the transmission amplitude via tunneling path cgb, etc. This can be seen more clearly in the situation $\theta_L = \theta_R = 0$, where we have $T_1^\uparrow = G^{r\uparrow\uparrow}\sqrt{(1+P)/2}\,T_1^L\sqrt{(1+P)/2}\,T_1^R e^{i\phi_{so}}$ and

$T_3^{\uparrow} = G^{r\downarrow\uparrow}\sqrt{(1+P)/2}\,T_3^L\sqrt{(1+P)/2}\,T_1^R e^{i\phi_{so}}$, which just correspond to paths ab and cgb. Here we list all the paths for $G^{\uparrow}$: $T_1^{\uparrow} \sim ab$, $T_2^{\uparrow} \sim cf$, $T_3^{\uparrow} \sim cgb$, $T_4^{\uparrow} \sim ahf$, $T_5^{\uparrow} \sim ae$, $T_6^{\uparrow} \sim cj$, $T_7^{\uparrow} \sim cge$, and $T_8^{\uparrow} \sim ahj$. The first four paths, which interfere with each other, correspond to the spin-up electrons tunnel to the spin-up states in the right lead, while the latter four correspond to the spin-up electrons tunnel to the spin-down states. Although there is no intradot coupling between the spin-up and down states in the dot, paths g and h still exist, which correspond to the transition through the leads [28]. For example, an electron tunnels via path g actually means that it tunnels from the spin-down state to the spin-up state in the dot via the left lead (paths ca and id), or via the right lead (paths je and fb). This can be seen from the expression of $G^{r\downarrow\uparrow}$, which describes path g. Here $G^{r\downarrow\uparrow}$ is proportional to $\Gamma_{12}(=\Gamma_{12}^{L\uparrow}+\Gamma_{12}^{L\downarrow}+\Gamma_{12}^{R\uparrow}+\Gamma_{12}^{R\downarrow})$ ($|\Gamma_{12}^{\alpha\sigma}| = \sqrt{\Gamma_{11}^{\alpha\sigma}\Gamma_{22}^{\alpha\sigma}}$), and these four terms just describe the four paths ca, id, je, and fb.

According to the parameters we set in Figures 2b and 2c, $T_1^{\uparrow}$, $T_3^{\uparrow}$, $T_6^{\uparrow}$, and $T_8^{\uparrow}$ contribute to $G^{\uparrow}$, while only $T_6^{\downarrow}$ contribute to $G^{\downarrow}$. Then we have $G^{\uparrow} = (1+P)^2\left|G^{r\uparrow\uparrow}T_1^LT_1^R + G^{r\downarrow\uparrow}T_3^LT_1^R\right|^2/4 + (1+P)(1-P)\left|G^{r\downarrow\downarrow}T_3^LT_1^R + G^{r\uparrow\downarrow}T_1^LT_1^R\right|^2/4$ and $G^{\downarrow} = (1-P)^2\left|G^{r\downarrow\downarrow}T_1^LT_1^R\right|/4$. So $G^{\downarrow}$ always shows a peak at ε_0. When P approaches 1, the first term in the expression of $G^{\uparrow}$ dominates, so the phenomenon revealed in Figure 2c is the result of the interference between paths ab and cgb. From the expression of G^r we see that at the resonant energy, the two paths have a phase difference π, so the interference produces the dip in the conductance spectra. When T_3^L/T_1^L approaches 1, $|T_3^{\uparrow}|$ gets closed to $|T_1^{\uparrow}|$, and the destructive interference becomes stronger. At non-resonant energy, the phase difference between $T_1^{\uparrow}$ and $T_3^{\uparrow}$ is smaller than π but still larger than $\pi/2$, so when we let $T_3^L > 0$, the additional path cgb always reduces $G^{\uparrow}$, especially at the resonant level. Further more, when we set $P = 1$, the two paths have exactly the same amplitude at ε_0, where completely destructive interference happens, which is shown in Figure 2d. Note that now $G^{\downarrow} = 0$ and $G = G^{\uparrow}$. This means that in strong polarization system, a weak spin-flip scattering can completely suppress the conductance at the resonant level. In fact, we have checked that when T_4^L and T_4^R are also finite, the behavior of both $G^{\uparrow}$ and $G^{\downarrow}$ still holds. But when T_3^R is non-zero at the same time, the situation becomes much different, which will be demonstrated later.

When the angle between the magnetizations of the two leads θ is finite, the dip in the conductance spectra still exists. In the inset to Figure 2d, we show the spectra of $G^{\uparrow}$ for $\theta = \pi$. With T_3^L increasing, the dip appears, but the value of $G^{\uparrow}$ increases with T_3^L. The reason is that the finite T_3^L rotates the magnetization of the left lead, which equivalently reduces the relative angle θ and increases the conductance. When Rashba SO coupling are taken into account, the conductance is suppressed, which is depicted in Figure 3a. We can see that as the Rashba phase ϕ_{so} increases from 0 to $\pi/2$, the dip at the resonant

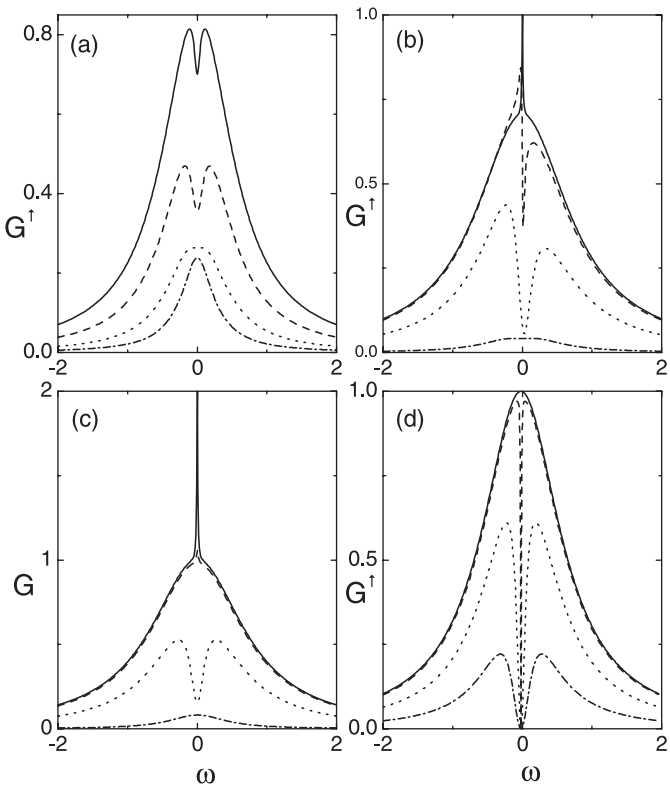

Fig. 3. Energy-resolved linear conductance G and $G^{\uparrow}$ under the influence of Rashba SO coupling. (a) $G^{\uparrow}$ for different Rashba phase factor ϕ_{so}. $P = 0.8$, $T_3^L = T_4^L = T_4^R = 0$, $T_3^R/T_1^L = 0.8$, $\theta_L = 2\pi/3$, and $\theta_R = 0$. (b) $G^{\uparrow}$ in the case of parallel leads with $P = 0.4$ and $T'/T = 0.8$, and the corresponding case for the total conductance G is shown in (c). (d) $G^{\uparrow}$ in the case of parallel leads with $P = 1$ and $T'/T = 0.6$. In (a) the solid, dashed, dotted, and dash-dotted lines correspond to $2\phi_{so} = 0, \pi/2, 3\pi/4$, and π, and in (b), (c), and (d) correspond to $2\phi_{so} = 0, \pi/8, \pi/2$, and π, respectively. For all figures $T_1^L = T_1^R = \sqrt{2}/2$ is assumed.

level changes to a flat peak, and the non-resonant part of the conductance is greatly reduced. This is because the Rashba SO coupling changes the relative phases between different paths, which can be seen from equation (14). So when the Rashba phase ϕ_{so} is altered, which can be realized by tuning the external electric field, the interferences between different paths are changed, thus the conductance spectra is tuned.

Next we investigate the situation that $T_3^L = T_4^L = T_3^R = T_4^R \equiv T'$, i.e., the magnetic impurities exist at both the left and right barriers, and have equal effects on spin-up and down electrons. Here we also assume $T_1^L = T_1^R \equiv T$, and we denote T^2 by Γ and T'^2/T^2 by γ. Figure 4a shows the conductance spectra for different γ when the magnetizations of the two leads are parallel. When $\gamma = 0$, equation (14) reduces to $G^{\uparrow} = [(1+P)^2\Gamma^2/4]/[(\omega-\varepsilon_0)^2 + (1+P)^2\Gamma^2/4]$, and $G^{\uparrow}$ has one full resonant peak at ε_0 with width $(1+P)\Gamma$, which is shown by the solid line in Figure 4a. As γ increases, the peak becomes broad, while there is a more narrow peak appears at ε_0, whose width decreases with γ. When $\gamma = 1$,

$$G^{\uparrow} \simeq \frac{(1+P)^2(1+\gamma)^2\Gamma^2/4+(1-P^2)\gamma\Gamma^2}{(\omega-\varepsilon_0)^2+(1+\gamma)^2\Gamma^2}+\frac{[(1+\gamma)^2-(1+P)^2(1+\gamma)^2/4-\gamma(1-P^2)](1-P^2)^2(1-\gamma)^4\Gamma^2/16(1+\gamma)^4}{(\omega-\varepsilon_0)^2+(1-P^2)^2(1-\gamma)^4\Gamma^2/16(1+\gamma)^2}, \tag{16}$$

$$G^{\uparrow} \simeq \frac{[(1+P)^2\gamma+(1-P^2)(1+\gamma)^2/2]\Gamma^2}{(\omega-\varepsilon_0)^2+4\gamma\Gamma^2}+\frac{[1-P^2-(1+P)^2\gamma/4-(1-P^2)(1+\gamma)^2/8](1-\gamma)^4\Gamma^2/64\gamma}{(\omega-\varepsilon_0)^2+(1-\gamma)^4\Gamma^2/64}. \tag{17}$$

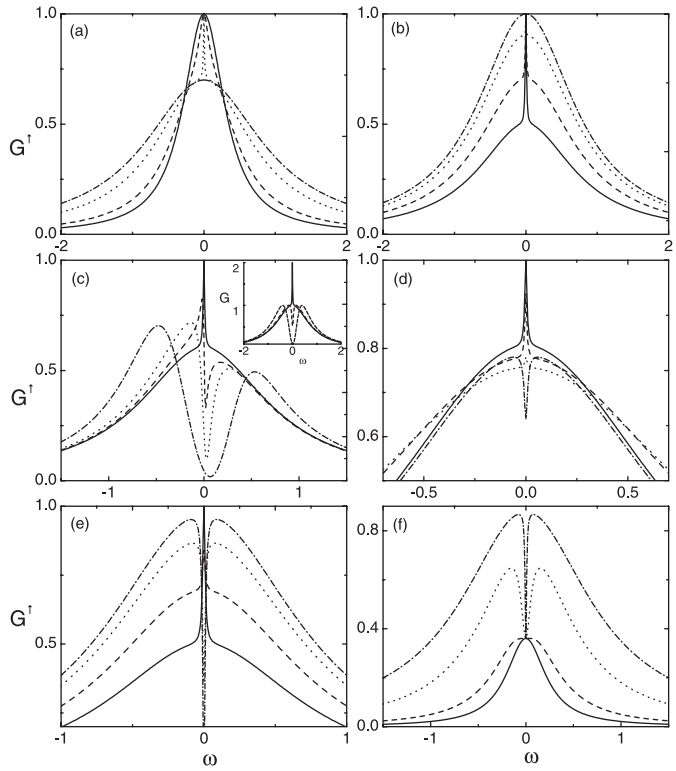

Fig. 4. Energy-resolved linear conductance G and $G^{\uparrow}$ for different sets of parameters in the absence of Rashba SO coupling. (a) $G^{\uparrow}$ for different T'/T in the case of $\theta_R = 0$ and $P = 0.4$. (b) $G^{\uparrow}$ for different lead polarizations P with $\theta_R = 0$ and $T'/T = 0.8$. (c) $G^{\uparrow}$ for different energy level spacing $\Delta\varepsilon$ in the case of $\theta_R = 0$, $P = 0.2$, and $T' = 0.8$. The inset shows the corresponding situation for total conductance G for $\Delta\varepsilon = 0, 0.3$, and 0.8, respectively. (d) $G^{\uparrow}$ for different relative magnetization angle θ with $P = 0.6$ and $T'/T = 0.8$. (e) $G^{\uparrow}$ for different P with $\theta_R = \pi$ and $T'/T = 0.8$. (f) $G^{\uparrow}$ for different T'/T when $\theta_R = \pi$ and $P = 0.8$. For all figures $\theta_L = 0$ and $T = \sqrt{2}/2$ are assumed. In (a)-(f) the solid, dashed, dotted, and dash-dotted lines correspond to $T'/T = 0, 0.4, 0.8, 1$, $P = 0, 0.4, 0.8, 1$, $\Delta\varepsilon = 0, 0.16, 0.4, 1$, $\theta_R = 0, \pi/4, \pi/2, \pi$, $P = 0, 0.4, 0.8, 1$, and $T'/T = 0, 0.2, 0.5, 0.8$, respectively.

we have $G^{\uparrow} = [2(1+P)\Gamma^2]/[(\omega-\varepsilon_0)^2+4\Gamma^2]$. Now the narrow peak disappears with the broad peak left, whose width and height are 4Γ and $(1+P)/2$, respectively. $G^{\downarrow}$ has the same features as $G^{\uparrow}$ so we don't present its figures here. Note that the similar phenomena had been discussed in [28], where the parameter α plays the same role as γ in our work. Compared with their results we know that the formation of the narrow peak is caused by the transition of electrons in the dot through the two leads, i.e., through paths g and h, which are introduced in by the finite T'. When γ approaches 1, all paths contribute to the conductance and have nearly the same amplitude. Then the interferences lead to the formation of the narrow peak. In fact, when γ gets closed to 1, equation (14) can be approximately written as

see equation (16) above.

which is composed of a broad peak with width $2(1+\gamma)\Gamma$ and a narrow peak with width $(1-P^2)(1-\gamma)^2\Gamma/[2(1+\gamma)]$. We plot $G^{\uparrow}$ for different P in Figure 4b, and we can see that the narrow peak appears when $G^{\uparrow}$ is just equal to $(1+P)/2$ (the vertex of the broad peak), and its width also decreases with P.

Once the level is no longer spin-degenerate, phase differences between paths at ε_0 appear, and the resonant peak is expected to be suppressed. This is depicted in Figure 4c. As the energy difference between the two states increases, the narrow peak in the spectra of $G^{\uparrow}$ soon reduces to a dip, and two lower peaks appear at $\varepsilon_{\uparrow}$ and $\varepsilon_{\downarrow}$. Because $T > T'$, the peak at $\varepsilon_{\uparrow}$ is higher than that at $\varepsilon_{\downarrow}$. In the inset the total conductance shows similar phenomenon, except that the resonant peak is split into two peaks with the same height.

When the magnetizations of the two leads are noncollinear, the situation becomes different, which is depicted in Figures 4d–4f. In Figure 4d we see that with the increasing of the relative angle θ, the broad peak still exists, while the narrow peak is suppressed and finally becomes an antiresonance when $\theta = \pi$. In fact, this phenomenon only happens when P is large, which can be seen in Figure 4e that when $\theta = \pi$, the narrow peak still exists for small P. The reason is that when P is small, the relative angle θ has little influence on transport properties. As P increases, the peak changes to an antiresonance. The detailed structure can be gained by rewriting equation (14) when $\theta = \pi$ and γ approached 1 as

see equation (17) above.

The second term corresponds to the narrow peak (dip). When γ gets closed to 1, the value of the narrow peak (dip) at ε_0 is $(P+1)(1-3P)$, which is negative when P is large. So we conclude that when P and θ are positive, the full transmission disappears, and when P and θ is large, the resonance can change to an antiresonance. Figure 4f plots $G^{\uparrow}$ as increasing γ when $\theta = \pi$. Now $G^{\uparrow}$ increases with γ, except at ε_0. When γ approaches 1, the antiresonance appears, which is similar to the case when $\theta = 0$.

When Rashba SO coupling is considered, each path gains an additional phase factor $e^{\pm i\phi_{so}}$, so the constructive

interference disappears and the resonant peak in Figure 4a is reduced. In Figure 3b we show that when ϕ_{so} increases from 0, the resonant peak is soon transformed to a dip, and two asymmetrical lower peaks appear beside it, which is similar to the case when the degeneracy of the level is broken. As ϕ_{so} keeps increasing, $G^{\uparrow}$ is further reduced, and when $2\phi_{so} = \pi$, the whole spectra is greatly suppressed. The corresponding situation for the total conductance is shown in Figure 3c, where we can see the suppression of the resonant peak more clearly. In Figure 3d we set $P = 1$. As we have stated, now the narrow peak vanishes, but the full transmission still exists. When ϕ_{so} is finite, the full transmission suddenly transforms to transmission zero, which indicates that the Rashba SO coupling generates phase differences between different paths, and changes the constructive interference into completely destructive interference.

Now we discuss the situation that the dot contains two energy levels, where the Rashba interlevel spin-flip effect must be taken into account. In fact, if the strength of Rashba interlevel spin-flip effect t is small compared to dot-lead coupling strength, all the phenomena we revealed in the single-level situation can be reproduced in the two-level situation. For instance, we give one figure corresponding to Figure 4a in the inset of Figure 5a. In the single-level system, the intralevel spin-flip effect is absent and the system is simply connected, while in the two-level system, owing to the interlevel spin-flip effect, the topological property of the system has been changed. To some extent the two-level system is similar to an Aharonov-Bohm interferometer with parallel-coupled double dots [29–31], where the Rashba phase factor plays the similar role to external magnetic flux. So we expect that the interplay between Rashba phase shift and Rashba spin-flip effect can produce some new phenomena which are absent in single-level situation.

Owing to the interlevel spin-flip effect, the number of the tunneling paths in the two-level system are much more than that in the single-level system. So the transmission amplitude picture is no longer convenient to describe such a system. Here we use the QD-molecule representation, which is achieved by diagonalizing the Hamiltonian of the dot:

$$H_d = \varepsilon_{1\uparrow} d_{1\uparrow}^{\dagger} d_{1\uparrow} + \varepsilon_{2\downarrow} d_{2\downarrow}^{\dagger} d_{2\downarrow} - t d_{1\uparrow}^{\dagger} d_{2\downarrow} - t d_{2\downarrow}^{\dagger} d_{1\uparrow} + \varepsilon_{1\downarrow} d_{1\downarrow}^{\dagger} d_{1\downarrow} + \varepsilon_{2\uparrow} d_{2\uparrow}^{\dagger} d_{2\uparrow} + t d_{1\downarrow}^{\dagger} d_{2\uparrow} + t d_{2\uparrow}^{\dagger} d_{1\downarrow}. \quad (18)$$

From this expression we know that we can diagonalize the parts of $(d_{1\uparrow}, d_{2\downarrow})$ and $(d_{1\downarrow}, d_{2\uparrow})$ separately. Applying two unitary transformation

$$\begin{pmatrix} d_{2\downarrow} \\ d_{1\uparrow} \end{pmatrix} = \begin{pmatrix} \cos\beta_1 & \sin\beta_1 \\ -\sin\beta_1 & \cos\beta_1 \end{pmatrix} \begin{pmatrix} d_{1+} \\ d_{1-} \end{pmatrix}, \quad \begin{pmatrix} d_{2\uparrow} \\ d_{1\downarrow} \end{pmatrix} = \begin{pmatrix} \cos\beta_2 & -\sin\beta_2 \\ \sin\beta_2 & \cos\beta_2 \end{pmatrix} \begin{pmatrix} d_{2+} \\ d_{2-} \end{pmatrix} \quad (19)$$

with $\beta_1 = \frac{1}{2}\arctan[2t/(\varepsilon_{2\downarrow} - \varepsilon_{1\uparrow})]$ and $\beta_2 = \frac{1}{2}\arctan[2t/(\varepsilon_{2\uparrow} - \varepsilon_{1\downarrow})]$, H_d is transformed to $H_d = \varepsilon_{1+} d_{1+}^{\dagger} d_{1+} + \varepsilon_{1-} d_{1-}^{\dagger} d_{1-} + \varepsilon_{2+} d_{2+}^{\dagger} d_{2+} + \varepsilon_{2-} d_{2-}^{\dagger} d_{2-}$, where

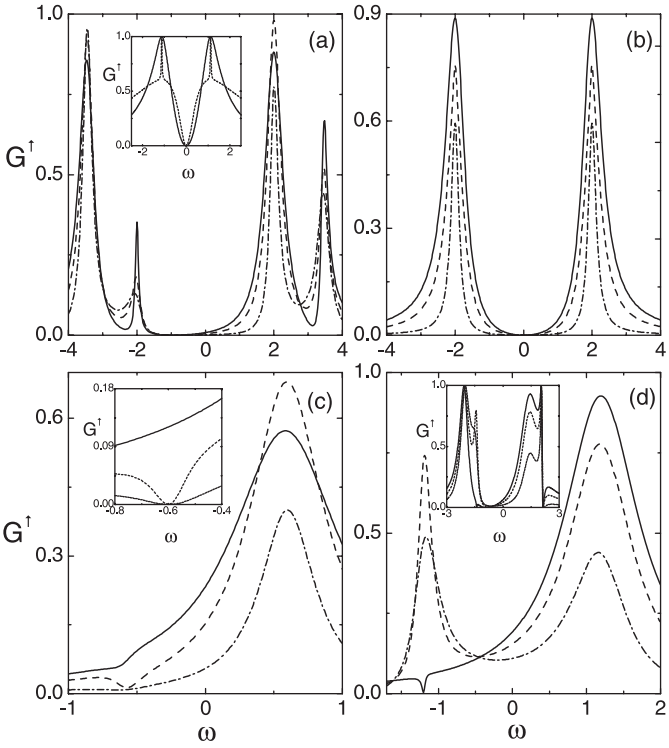

Fig. 5. Energy-resolved linear conductance $G^{\uparrow}$ in system with two energy levels under the influence of Rashba SO coupling. The solid, dashed, and dash-dotted lines correspond to $2\phi_{so} = 0, \pi/2$, and π, respectively. (a) $G^{\uparrow}$ in the case of non-degenerate energy levels ($\varepsilon_{1\uparrow} = -\varepsilon_{2\downarrow} = -3$ and $\varepsilon_{1\downarrow} = -\varepsilon_{2\uparrow} = -1$) when $\theta_L = \theta_R = \pi/2$, $P = 0.8$, $t = \sqrt{3}$, $T_{11}^{L} = T_{21}^{L} = 0.5$, $T_{11}^{R} = T_{21}^{R} = 1/\sqrt{2}$, and $T_{n2}^{\alpha} = T_{n3}^{\alpha} = 0$. The corresponding case for degenerate levels ($\varepsilon_{1\uparrow} = \varepsilon_{1\downarrow} = -1$ and $\varepsilon_{2\uparrow} = \varepsilon_{2\downarrow} = 1$) is shown in (b). The inset shows the two-level case corresponding to Figure 4a, where we set $\varepsilon_{1\uparrow} = \varepsilon_{1\downarrow} = -1$, $\varepsilon_{2\uparrow} = \varepsilon_{2\downarrow} = 1$, $P = 0.2$, $t = 0.5$, $T = 1$, and $T' = 0.2$ and 0.8. (c) $G^{\uparrow}$ in the case that $1\pm$ states are decoupled from the system. $\varepsilon_{1\downarrow} = -\varepsilon_{2\uparrow} = -0.3$, $\theta_L = \theta_R = 0$, $P = 0.4$, $t = 0.3\sqrt{3}$, $T_{12}^{\alpha} = T_{21}^{\alpha} = 1/\sqrt{3}$, and $T_{13}^{\alpha} = T_{24}^{\alpha} = 1/3$. The inset shows the corresponding situation for $P = 1$. (d) The same case with (c), except that $\varepsilon_{1\downarrow} = -\varepsilon_{2\uparrow} = -0.6$, $\theta_L = \pi/2$, $\theta_R = 0$, $P = 1$ and $t = 0.6\sqrt{3}$. The inset shows the case when $1\pm$ states are coupled to the system again, where $\varepsilon_{1\uparrow} = -1.7$, $\varepsilon_{1\downarrow} = -0.7$, $\varepsilon_{2\uparrow} = 0.7$, and $\varepsilon_{2\downarrow} = 1.7$.

$\varepsilon_{1\pm} = \left(\varepsilon_{1\uparrow} + \varepsilon_{2\downarrow} \pm \sqrt{(\varepsilon_{2\downarrow} - \varepsilon_{1\uparrow})^2 + 4t^2}\right)/2$ and $\varepsilon_{2\pm} = \left(\varepsilon_{1\downarrow} + \varepsilon_{2\uparrow} \pm \sqrt{(\varepsilon_{2\uparrow} - \varepsilon_{1\downarrow})^2 + 4t^2}\right)/2$ are the renormalized energy levels. When the system is spin-degenerate, i.e., $\varepsilon_{1\uparrow} = \varepsilon_{1\downarrow}$ and $\varepsilon_{2\uparrow} = \varepsilon_{2\downarrow}$, we also have $\varepsilon_{1+} = \varepsilon_{2+}$ and $\varepsilon_{1-} = \varepsilon_{2-}$, since the Rashba interlevel spin-flipping doesn't break the spin-degeneracy. The corresponding tunneling Hamiltonian is $H_{T\alpha} = \sum_{k_\alpha \sigma \xi} [T_{\xi}^{\alpha\sigma} a_{k_\alpha \sigma}^{\dagger} d_{\xi} + H.c.]$ ($\xi = 1\pm, 2\pm$), and the coupling coefficients are $T_{1+}^{\alpha\sigma} = -\widetilde{T}_{\alpha 1}^{\sigma\uparrow} \sin\beta_1 + \widetilde{T}_{\alpha 2}^{\sigma\downarrow} \cos\beta_1$, $T_{1-}^{\alpha\sigma} = \widetilde{T}_{\alpha 1}^{\sigma\uparrow} \cos\beta_1 + \widetilde{T}_{\alpha 2}^{\sigma\downarrow} \sin\beta_1$, $T_{2+}^{\alpha\sigma} = \widetilde{T}_{\alpha 2}^{\sigma\uparrow} \cos\beta_2 + \widetilde{T}_{\alpha 1}^{\sigma\downarrow} \sin\beta_2$, and $T_{2-}^{\alpha\sigma} = -\widetilde{T}_{\alpha 2}^{\sigma\uparrow} \sin\beta_2 + \widetilde{T}_{\alpha 1}^{\sigma\downarrow} \cos\beta_2$. Notice that different from the single-level case, now the Rashba phase doesn't enter these coupling

coefficients as an integer phase factor. For example, $T_{2+}^{\alpha\uparrow} = -[T_{21}^{\alpha}\cos(\theta_\alpha/2) + T_{24}^{\alpha}\sin(\theta_\alpha/2)]\cos\beta_2 e^{-i\phi_{so}^{\alpha}} + [T_{13}^{\alpha}\cos(\theta_\alpha/2) + T_{12}^{\alpha}\sin(\theta_\alpha/2)]\sin\beta_2 e^{i\phi_{so}^{\alpha}}$. Because $\left|T_{\xi}^{\alpha\sigma}\right|^2$ is the coupling strength between the αth lead and the ξth level for electrons with spin σ, the Rashba phase factor can modulate the width and height of the peak at ε_ξ in the spectra of G^σ via tuning $T_{\xi}^{\alpha\sigma}$, which is shown in Figures 5a and 5b. This effect is absent in the single-level system because of its simple topological structure. In Figure 5a the four levels are chosen to be non-degenerate, which is realized by applying an external field through the dot. We see that the Rashba phase can modulate both the width and height of the four peaks in the spectra of $G^\uparrow$, owing to the interlevel spin-flip effect. When the external magnetic field is absent, the spin-degeneracy is recovered and the four renormalized levels merge to two, as depicted in Figure 5b. Now the details of each peak are smeared because of the superposition of $1+$ $(1-)$ and $2+$ $(2-)$ states.

At last we investigate some specific systems, where the Rashba SO coupling can cause some interesting effects. For clarity, we first let the states $1\pm$ be decoupled from the system ($T_{1\pm}^{\alpha\sigma} = 0$). Now only $2+$ and $2-$ states are coupled to the two leads. For specific setting of system parameters we can make $T_{2-}^{L\uparrow} = T_{2-}^{R\uparrow} = 0$ when $\phi_{so} = 0$. Now for spin-up electrons, $2-$ state is also decoupled from the system, so there is only one resonant peak at ε_{2+} in $G^\uparrow$ (see the solid line in Fig. 5c). When ϕ_{so} increases, $T_{2-}^{L\uparrow}$ remains zero, while $T_{2-}^{R\uparrow}$ is no longer zero. So now the $2-$ state is side-coupled to the system via the right lead, and the electrons can tunnel through the structure via two paths. The first one is directly tunneling into the right lead through $2+$ state, and the second is first tunneling through $2+$ state, and then tunneling onto and out of $2-$ state and finally into the right lead. There is a phase difference of π between these two paths, because when electron with energy ε_{2-} tunnels onto and out of $2-$ state, it gains a phase shift of π [32–35]. So the destructive interference causes a dip in $G^\uparrow$ at ε_{2-} when $\phi_{so} > 0$, as we can see in Figure 5c. The dip at ε_{2-} doesn't reduce to zero, because the spin-down electrons also contribute to $G^\uparrow$ through the matrix $\Gamma^{\alpha\downarrow}$. If we choose $P = 1$, the contribution from spin-down electrons $\Gamma^{\alpha\downarrow}$ disappears, and completely destructive interference can happen at ε_{2-}, which is shown in the inset of Figure 5c. Similarly we plot Figure 5d, where we choose the parameters to make $T_{2-}^{L\uparrow} > 0$ and $T_{2-}^{R\uparrow} = 0$ when $\phi_{so} = 0$, so now $2-$ state is side-coupled to the system and the dip appears. As ϕ_{so} increasing, $T_{2-}^{R\uparrow}$ is also finite, and electrons can tunnels to the right lead directly through $2-$ state, which produces the resonant peak at ε_{2-}. So the Rashba phase can transform the transmission zero into resonance peak. When $1\pm$ states are coupled to the system again, the behavior of $G^\uparrow$ at $\varepsilon_{2\pm}$ stated above still holds, provided that the four states are not degenerate. This is shown in the inset of Figure 5d. Besides, we can see in Figure 5d that the interferences between the tunneling paths through the four states produce Fano resonant structures at ε_{1-} and ε_{2+}. Because ε_{2-} is most closed to ε_{1-}, the Fano resonance at ε_{1-} is mainly caused by interference between the paths through $2-$ and $1-$ states. From the expression of $T_{\xi}^{\alpha\sigma}$ we know that $T_{1+}^{\alpha\sigma} \simeq T_{2-}^{\alpha\sigma}$ and $T_{1-}^{\alpha\sigma} \simeq T_{2+}^{\alpha\sigma}$. According to reference [29], the level with strong coupling strength to the leads serves as the reference channel, and the Fano resonance shows up at the level with weak coupling strength. So when we have $|T_{1-}^{\alpha\sigma}| \ll |T_{2-}^{\alpha\sigma}|$, the Fano resonances appear at ε_{1-} and ε_{2+}, and the Breit-Wigner resonances appear at ε_{1+} and ε_{2-}, as shown in the inset of Figure 5d. If the spin-degeneracy is recovered, $1\pm$ states will be superposed with $2\pm$ states, and the phenomena would be smeared.

In summary, we have investigated the spin-dependent linear conductance spectra of a FM/QD/FM tunneling system in the presence of both spin-flip scattering and Rashba SO coupling. In the single-level system, it is found that there could be a narrow peak or dip at the resonant level, which is the result of spin-flip scattering. The Rashba SO coupling can change the interference pattern and greatly suppress the conductance. In the two-level system, the Rashba interlevel spin-flipping makes the topology of the structure different from that of the single-level system, and its interplay with Rashba phase shift can tune the coupling strengths between the leads and the renormalized levels. Thus, both the width and height of the resonant peaks are modulated by the Rashba phase shift, and in some specific system even the transition from resonance to antiresonance can occur.

The authors are grateful to Prof. Qing-Feng Sun for his helpful discussions. This project was supported by the National Natural Science Foundation of China (No. 10474052), by Tsinghua Basic Research Foundation (No. JCpy2005058), by Specialized Research Fund for the Doctoral Program of Higher Education (No. 2006003047), and by the National Key Project of Basic Research Development Plan (No. 2006CB605105).

References

1. M.N. Baibich, J.M. Broto, A. Fert, F.N.V. Dau, F. Petroff, P. Eitenne, G. Creuzet, A. Friederich, J. Chazelas, Phys. Rev. Lett. **61**, 2472 (1998)
2. G. Binasch, P. Grünberg, F. Saurenbach, W. Zinn, Phys. Rev. B **39**, 4828 (1989)
3. W.P. Pratt, Jr, S.-F. Lee, J.M. Slaughter, R. Loloee, P.A. Schroeder, J. Bass, Phys. Rev. Lett. **66**, 3060 (1991)
4. S.A. Wolf, D.D. Awschalom, R.A. Buhrman, J.M. Daughton, S. von Molnár, M.L. Roukes, A.Y. Chtchelkanova, D.M. Treger, Science **294**, 1488 (2001); Igor Žutić, Jaroslav Fabian, S. Das Sarma, Rev. Mod. Phys. **76**, 323 (2004)
5. J.C. Slonczewski, Phys. Rev. B **39**, 6995 (1989)
6. M. Reed, Scientific American **268**, 118 (1993)
7. M. Kastner, Physics Today **46**, 24 (1993)
8. G. Schön, A.D. Zaikin, Phys. Rep. **198**, 237 (1990); C.W.J. Beenakker, Phys. Rev. B **44**, 1646 (1991)
9. Y. Nagamune, H. Sakaki, L.P. Kouwenhoven, L.C. Mur, C.J.P.M. Harmans, J. Motohisa, H. Noge, Appl. Phys. Lett. **64**, 2379 (1994)
10. L.I. Glazman, R.I. Shekhter, J. Phys.: Condens. Matter **1**, 5811 (1989)

11. L.P. Kouwenhoven, N.C. van der Vaart, A.T. Johnson, W. Kool, C.J.P.M. Harmans, J.G. Williamson, A.A.M. Staring, C.T. Foxon, Z. Phys. B **85**, 367 (1991)
12. S. Datta, B. Das, Appl. Phys. Lett. **56**, 665 (1990)
13. E.I. Rashba, Sov. Phys. Solid State **2**, 1109 (1960); Yu. A. Bychkov, E.I. Rashba, J. Phys. C **17**, 6093 (1984)
14. J. Nitta, T. Akazaki, H. Takayanagi, T. Enoki, Phys. Rev. Lett. **78**, 1335 (1997)
15. D. Grundler, Phys. Rev. Lett. **84**, 6074 (2000)
16. S. Murakami, N. Nagaosa, S.C. Zhang, Science **301**, 1348 (2003)
17. J. Sinova, D. Culcer, Q. Niu, N.A. Sinitsyn, T. Jungwirth, A.H. MacDonald, Phys. Rev. Lett. **92**, 126603 (2004)
18. I. Weymann, J. König, J. Martinek, J. Barnaś, G. Schön, Phys. Rev. B **72**, 115334 (2005)
19. W. Rudziński, J. Barnaś, Phys. Rev. B **64**, 085318 (2001)
20. W. Rudziński, J. Barnaś, R. Świrkowicz, M. Wilczyński, Phys. Rev. B **71**, 205307 (2005)
21. P. Zhang, Q.K. Xue, Y.P. Wang, X.C. Xie, Phys. Rev. Lett. **89**, 286803 (2002)
22. T.P. Pareek, Phys. Rev. B **66**, 193301 (2002)
23. Qing-Feng Sun, Jian Wang, Hong Guo, Phys. Rev. B **71**, 165310 (2005)
24. Z.G. Zhu, G. Su, Q.R. Zheng, B. Jin, Phys. Lett. A **300**, 658 (2002)
25. A. Vedyayev, R. Vlutters, N. Ryzhanova, J.C. Lodder, B. Dieny, Eur. Phys. J. B **25**, 5 (2002)
26. Zhen-Gang Zhu, Gang Su, Qing-Rong Zheng, Biao Jin, Phys. Rev. B **70**, 174403 (2004)
27. A.-P. Jauho, N.S. Wingreen, Y. Meir, Phys. Rev. B **50**, 5528 (1994); H. Haug, A.-P. Jauho, *Quantum Kinetics in Transport and Optics of Semiconductors* (Springer-Verlag, Berlin, 1996)
28. T.V. Shahbazyan, M.E. Raikh, Phys. Rev. B **49**, 17123 (1994)
29. H.Z. Lu, R. Lü, B.F. Zhu, Phys. Rev. B **71**, 235320 (2005)
30. K. Kang, S.Y. Cho, J. Phys.: Condens. Matter **16**, 117 (2003)
31. Z.M. Bai, M.F. Yang, Y.C. Chen, J. Phys.: Condens. Matter **16**, 2053 (2004)
32. A. Yacoby, M. Heiblum, D. Mahalu, H. Shtrikman, Phys. Rev. Lett. **74**, 4047 (1995)
33. Z.B. He, Y.J. Xiong, Phys. Lett. A **349**, 276 (2006)
34. J.F. Feng, X.F. Jiang, J.L. Zhong, S.S. Jiang, Physica B **365**, 20 (2005)
35. M. Tolea, B.R. Bulka, Phys. Stat. Sol. B **243**, 251 (2006)